CoA Note No.60

~~CONFIDENTIAL~~

THE COLLEGE OF AERONAUTICS

CRANFIELD

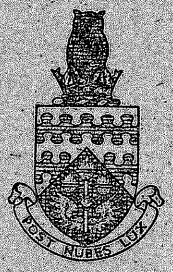

INTERFERENCE OF A REARWARD FACING JET ON THE FLOW OVER THREE REPRESENTATIVE AFTERBODY SHAPES

by

A. H. CRAVEN

MINISTRY OF SUPPLY CONTRACT 7/GEN/1473/PR3

CONFIDENTIAL

~~CONFIDENTIAL.~~

NOTE NO. 60

APRIL, 1957.

THE COLLEGE OF AERONAUTICS

CRANFIELD

The interference of a rearward facing jet on the flow over three representative afterbody shapes in a uniform subsonic flow

- by -

A. H. Craven, M.Sc., Ph.D., D.C.Ae.

SUMMARY.

This report contains the results of an experimental investigation into the interference of a rearward facing undeflected jet on the flow over three afterbody shapes at subsonic speeds. The tests were performed at a Reynolds number of 0.3×10^6 based on body diameter.

It was found that the form (or pressure) drag coefficient of the bluff afterbody of a right cylinder increased appreciably with increase in jet thrust coefficient. A similar but much smaller increase in form drag was found on an ellipsoidal afterbody and a 'boat-tail'.

The effect of the jet was found to extend to approximately three body diameters upstream of the jet exit but that beyond one body diameter the effect was very small.

Prepared under Ministry of Supply Contract 7/Gen/1473/PR3

CONTENTS.

LIST OF SYMBOLS.

C_D	form drag coefficient
C_J	jet thrust coefficient $\left(= \dfrac{mv_b}{\frac{1}{2}\rho U_o^2 S}\right)$
C_p	pressure coefficient $\left(= \dfrac{p - p_o}{\frac{1}{2}\rho U_o^2}\right)$
d	body diameter
l	distance from jet exit in upstream direction
m	jet mass flow
p	static pressure (suffix 'o' denotes value in freestream)
r	radial distance from jet centre
R	radius of body
S	base area $(= \pi R^2)$
U_o	free stream speed
v_b	equivalent jet velocity. (jet velocity attained in a isentropic expansion from jet stagnation pressure to freestream static pressure.)
ρ	air density

1. Introduction.

The treatment of the aerodynamic problems associated with the use of jet engines has been restricted, in the main, to investigations of the flow in and around intake ducts. Considerably less information can be found concerning the jet flow and its effect on the flow over the afterbody. This problem includes not only turbojet engine exhausts but also the rocket efflux from a missile and the design of the afterbody to give least drag.

In the past most work on jet flow, both theoretical and experimental, has been confined to the free jet and to the problem of the flow in the mixing region downstream of the jet exit. A recent paper by Cortright (1) contains some general information on the drag characteristics of boattails at one supersonic speed. A theoretical investigation into the effect of the jet on the flow over an afterbody is given by Craven (2). The latter treatment is however restricted to subsonic inviscid flow in which the difference between jet and mainstream speeds is small.

This paper presents the results of experiments to determine the effect of the undeflected jet upon the pressure distribution around three representative afterbodies in a uniform subsonic flow and the effect of the afterbody shape on the base drag of the body. Where applicable the theoretical results derived by the methods of reference 2 are compared with the experimental findings.

The experiments described here are part of a fuller investigation into the effect of jet flow sponsored by the Ministry of Supply under Contract No. 7/Gen/1473/PR3.

The effect of jet deflected on the flow over bodies at incidence will be the subjects of further reports.

2. Apparatus.

2.1. The Wind Tunnel.

The tests were performed in a straight-through wind tunnel having a closed working section measuring 3 ft. square. The compressed air supply for the jet was led into the settling chamber of the wind tunnel through a 4 in. diameter pipe enclosed in a streamlined fairing (fig.1). The supply pipe, of 3.5 in. diameter, continued along the centre line of the tunnel to the working section and was threaded at its downstream end to take the model (fig.2). The supply pipe was encased in a duralumin sleeve 4" in diameter, the space between the sleeve and supply pipe being occupied by the pressure tubes.

2.2. The models.

The three models tested were

(i) a right cylinder, 4" diameter and 12" long (fig.3a).

(ii) a cylinder tapering from 4" to $\frac{3}{4}$" diameter in a length of 9" giving a boat-tail angle of $10\frac{1}{4}^{\circ}$ (fig.3b).

(iii) an ellipsoid with semi-major and semi-minor axes 12" and 2" respectively (fig.3c).

The models were turned from light alloy. The internal cavity of each model was machined to give a smooth internal flow into a parallel-sided jet $\frac{3}{4}$" in diameter issuing from the model along its centre line. A gauze screen was fitted to damp disturbances and to eliminate non-uniformities in the compressed air flow from the supply pipe into the model cavity (fig.2).

Polythene tubing for pressure measurements was let into slots along the models' generators at angular intervals of $22\frac{1}{2}^{\circ}$ and secured with araldite. Pressure tappings were also fitted in the jet nozzle and in the compressed air supply pipe on both sides of the gauze screen. All these pressure tubes are taken out of the tunnel through the fairing of the supply pipe.

2.3. Instruments.

The tunnel speed was calculated from the pressure difference between pitot and static tubes of a standard pitot static tube as measured by a vertical Chattock manometer. The jet mass flow was measured by a vertical water manometer connected across a standard orifice plate. The jet and supply pipe pressures were measured on mercury manometers. The surface pressures were read from a multitube alcohol manometer.

Flow patterns on the models were photographed using an Exacta reflex camera, Ilford FP3 film and flash equipment.

3. Scope of tests.

The tests on each of the models covered a range of free stream speeds from 0 to 120 f.p.s and a range of "equivalent" jet speeds from 0 to 1500 f.p.s. The equivalent jet speed is that calculated from the jet blowing pressure assuming isentropic expansion to free stream pressure.

Defining the thrust coefficient C_J by.

$$C_J = \frac{m\, v_b}{\frac{1}{2}\rho U_o^2 S}$$

where m = jet mass flow (slug/sec)
v_b = equivalent jet speed (ft/sec)
U_o = tunnel speed (ft/sec)
S = base area of model (sq/ft)

the range of jet thrust coefficient covered by these tests was

$$0 \leqslant C_J \leqslant 40$$

4. Test Procedure.

4.1. Preliminary tests.

Before pressure measurements were made on any model, a set of pitot traverses were performed across the jet orifice to ensure uniform flow from the jet. This ensured that the same jet blowing pressure produced similar effects at the jet exit of each model.

4.2. Pressure plotting.

For every set of pressure tappings drilled, the tunnel speed was set at each of 0, 50, 80, 100, 120 f.p.s. For each tunnel speed the pressure at each tapping was measured at each of fifteen equivalent jet speeds covering the range 0 - 1500 f.p.s. Due to the entrainment by the jet, the tunnel speed had to be corrected after each alteration of jet speed.

Pressure measurements were made at intervals of 0.1" along the generators for the first two inches of the models length, at 0.2" intervals for the next two inches and at intervals of 0.5" for the remainder of the twelve inch body length. The above measurements were repeated for 16 angular positions around the body circumference. On the right cylindrical model measurements of pressure were also made at intervals of 0.1" on the basic radii.

4.3. Flow visualisation.

To determine the nature of the flow round the afterbodies, each was coated with a mixture of lampblack and light oil (Shell Vitrea 300). After a few minutes running, the resulting flow pattern was photographed.

5. Results.

5.1. Presentation of results.

It was found that the pressure coefficients at any point and drag coefficient for the four different tunnel speeds could be expressed uniquely in terms of C_J, the non-dimensional thrust parameter (see section 3).

The following graphs are given of pressure coefficient plotted against position (expressed non-dimensionally) for values of C_J from 0 to 40 : -

(i) pressure distribution on the base of the right cylinder (fig.4a).

(ii) pressure distribution on the side of the right cylinder (fig.4b).

(iii) pressure distribution on the side of the tapered afterbody (fig.5).

(iv) pressure distribution on the side of the ellipsoidal body (fig.6).

In addition these pressures have been resolved in the drag direction and integrated. The variation of the pressure drag coefficient with C_J for each of the three afterbodies is given in fig.7.

The important features found in the flow visualisation experiments are shown in figs. 8, 9 and 10. The details are as follows :-

fig. 8. Base of right cylinder : $C_J = 0$, $U_o = 120$ f.p.s.

fig. 9. Tapered afterbody : $C_J = 0$, $U_o = 120$ f.p.s.

fig.10. Tapered afterbody : $C_J = 5$, $U_o = 120$ f.p.s.

Some comparison with the theory of ref.2 is given in figs. 11 and 12.

5.2. The Pressure Distributions.

In all the tests made on these models it was found that the pressure distributions were cylindrically symmetric.

5.2.1. The right cylinder.

5.2.1.1. The base pressure distribution (fig.4a).

It is seen that the suction over the base increases as C_J increases and that the major increase occurs at the larger values of the base radius. Furthermore the pressure changes rapidly, for a given value of C_J, at about 0.6 of the base radius. At and near this base radius the suction decreases sharply only to recover and increase slightly before decreasing smoothly to its value at the outer base radius.

One feature has been omitted from fig. 4a in order to avoid confusion. With the jet overchoked the base suction was reduced by approximately ten per cent of its value when the jet was choked and thereafter remained constant.

5.2.1.2. The side pressure distribution (fig. 4b).

It is seen that, as on the base, the presence of the jet increases the slight suction on the side of the body. Two features are noteworthy. Firstly, as would be expected, the pressure at the corner with the base (i.e. $l/d = 0$) is equal to that obtained by extrapolation to $r/R = 1$ of the base pressure distribution for the same C_J. Secondly that the effect of the jet becomes negligible at some three to four body diameters upstream of the base.

The side pressure distribution for the overchoked jet coincided with the distribution for the choked jet.

5.2.2. The straight-tapered afterbody (Boat-tail) (fig.5).

With no jet, the distribution of pressure on the boat-tailed afterbody shows a peak suction at the shoulder. It also shows a boundary layer separation at 0.7 d upstream of the jet exit. There is also a region of constant pressure over the first 0.2 d upstream of the jet exit.

For all values of C_J increase of C_J increases the suction on the body except for when the jet is overchoked. It is noted that for moderate values of C_J (up to 20) the separated region from 0.7 d to 0.3 d

still exists but at higher values of C_J the flow characteristics change suddenly at 0.7 d. Furthermore it is only between the orifice and 0.7 d that there is any large change in pressure due to the presence of the jet. At distances greater than two body diameters up the body, the jet has no effect on the pressure distribution. Overchoking caused a slight reduction of motion from 0 to 0.2 d but had no effect on the pressure distribution further upstream.

5.2.3. The ellipsoidal afterbody (fig.6).

It is seen again that the body motion increases with the value of C_J and the presence of the jet has little effect at points further than three body diameters upstream of the jet exit. There is no evidence of separation on the body. On the other hand there is a sudden decrease in suction very close to the jet exit as the surface slope of the body increases rapidly towards the orifice. An effect due to overchoking similar to that found on the boat-tail is found on the ellipsoidal afterbody.

5.3. The Drag Coefficients (fig.7).

From integrations of the resolved pressures in the drag direction the afterbody pressure drag coefficients, based on body cross-sectional area, have been calculated and are plotted in figure 7. It is found that the value of C_D increases with C_J. The boat-tail has the least drag for a given C_J although its variation from that of the ellipsoidal afterbody is small. The right cylinder shows a very large base drag (the side pressures naturally make no contribution).

With the jet overchoked, the drag coefficient of the right cylinder was found to be reduced to approximately 90% of its value with the jet just choked. A similar effect was indicated for the other two afterbodies but not of sufficient magnitude to be visible in fig. 7.

5.4. Theoretical results.

The vorticity distributions representing the afterbody and jet were calculated for the cases of the boat-tail and the ellipsoid using the results of a slender body approach given in ref.2.

The corresponding pressure distributions were calculated for both shapes when $C_J = 0$ and 5. These pressure distributions are shown in comparison with the corresponding experimental results in figs. 11 and 12.

6. Discussion.

6.1. Accuracy of results.

The blowing pressure was set, by continual adjustment of the control valve, during any test to an accuracy better than 2.5%. The tunnel speed could be kept constant to within 1% and the surface pressures measured to 0.02 in of alcohol. Hence the overall error in the pressure coefficients is less than 5%.

No account has been taken of tunnel interference effects. It is considered that any errors from this cause are small since the jet was aligned along the centreline of the tunnel and the tunnel speed was adjusted to its prescribed value as the jet speed was altered and before any pressure readings were taken.

6.2. Entrainment effects.

The fact that the major pressure changes are found close to the jet exit indicates that they are due to the increase in speed of the flow over the rear surfaces caused by the entrainment, by the jet, of the mainstream flow (jetsink effect). It is also found that the entrainment affects the boundary layer only at points close to the jet exit. This is shown particularly in fig. 5 where a region of separated flow exists on the tapered afterbody even for moderate values of C_J. Close to the jet exit however there is a reattachment of flow attributed to entrainment (fig.10) and an accompanying increase in suction (fig.5).

Pitot traverse measurements in the wake confirm this reattachment since they show a normal mixing region with the jet on, whereas with no jet separation is apparent over an area larger than that of the jet orifice.

Similar large increases in the speed of flow near the rear end of the ellipsoidal afterbody are attributed to entrainment effects. In this connection it is assumed that the flow may separate very close to the jet exit where the surface slope becomes very large even though there is a large entrainment effect.

Pitot traverse measurements close to the jet exit indicate that the mixing region does not start exactly at the lip of the jet and that a small separated region exists there. From fig. 6 and from the pitot traverse measurements it is obvious that such a region of

separation is very small and appears to occur only at the higher blowing pressures.

6.3. The base pressure on the right cylinder.

The flow over the base of the right cylinder with no jet is completely separated and the base pressure is constant.

With the jet on there is no direct interaction between the jet and the free stream immediately at the base, the mixing region forming at between three and four body diameters downstream of the jet exit. However to obtain the high suctions shown in fig. 4a there must be an appreciable attached flow over the base and since the pressure distributions of fig. 4a are reproduced along each base radius, this flow must be radial. Furthermore there must be some form of stagnation line (with a stagnation pressure below that of the mainstream) at approximately 0.6R. Examination of flow patterns, of which fig. 8 is typical, indicates that there are in fact two circulating flows downstream of the base. It is noted that between 0.2R and 0.5R the flow on the face is towards the jet and from 0.7R to R the flow is outwards. This evidence together with the indication of a reversed flow derived from yawmeter tests in the region just downstream of the base suggest the presence of a pair of stationary toroidal vortices extending about three body diameters downstream of the base.

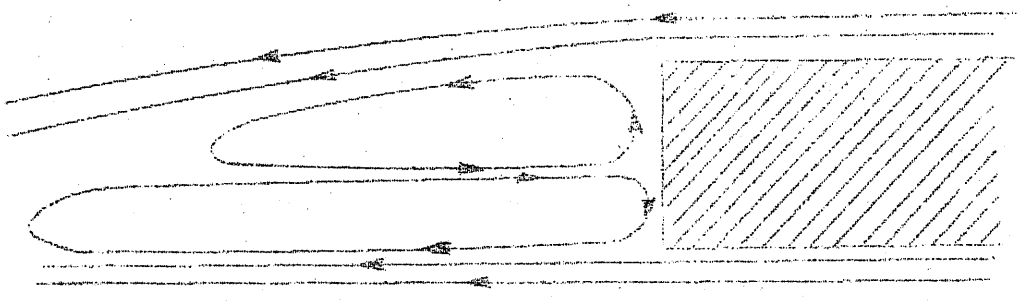

The energy required to maintain these vortices accounts for the very large increase in the base drag of the bluffended afterbody.

6.4. Comparison with theory.

The comparison between theory and experiment as shown in figure 11 and 12 is disappointing but it must be remembered that the theory used (reference 2) is a slender body theory, and that it strictly only applies to cases of small differences between the speeds of the jet and mainstream. Furthermore it takes no account of the entrainment (sink effect) between jet and stream which affects greatly the external flow particularly over the boat-tail. However even if the entrainment effect is included, the theory cannot include the separations of flow occuring on the boat-tail.

No comparison has been made for the bluff afterbody since the theory cannot be extended to bluff bases with large regions of separated flow.

7. Acknowledgement.

Thanks are due to Mr. S. H. Lilley for the design and erection of the blowing rig, to Mr. H. Stanton for the manufacture of the models and to Mr. D. Pollard, who together with other laboratory assistants, was largely responsible for taking the experimental measurements.

8. Conclusions.

(i) The effect of the jet is to increase the suction over the afterbody.

(ii) The major effects of the jet are limited to a region extending approximately one body diameter upstream of the jet exit.

(iii) Boat-tailing or streamlining the afterbody greatly reduces the form drag.

(iv) The large increase in the base drag of the right cylinder is due to the presence of a pair of toroidal vortices between the jet and the free stream.

(v) The existing theory does not predict the pressure distribution at all accurately and can only be used to suggest trends.

9. References.

1. Cortright, Edgar M., Nozzle - Afterbody Characteristics, Aeronautical Engineering Review, Sept. 1956.

2. Craven, A.H., A potential flow model for the flow about a nacelle with jet; College of Aeronautics Report No. 101, March 1956.

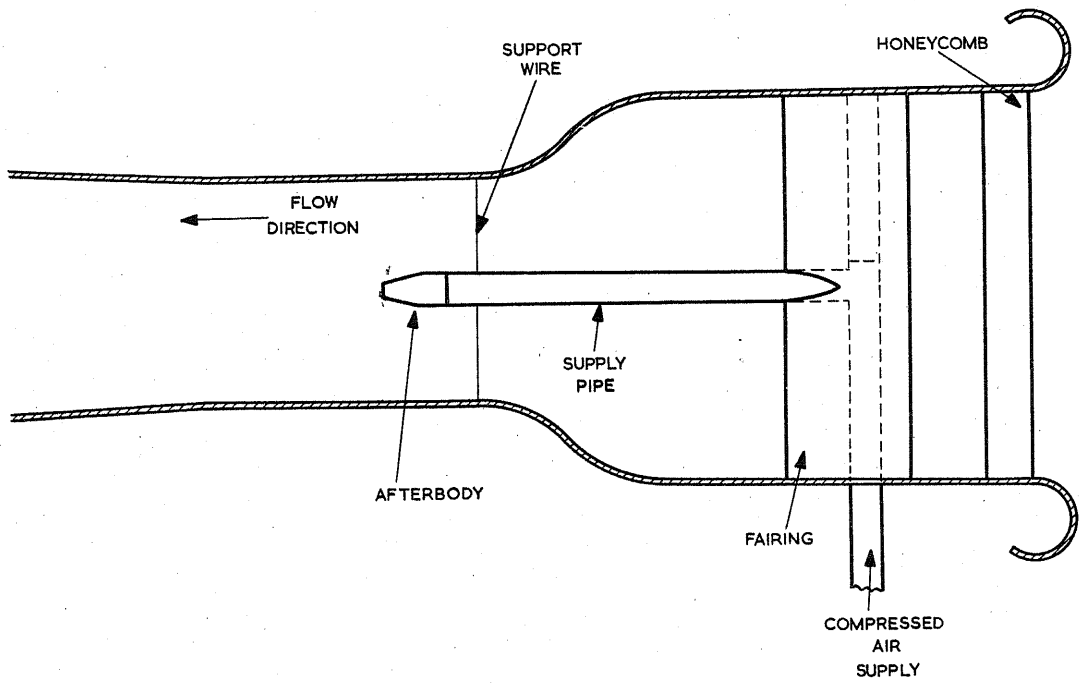

FIG. I.

GENERAL ARRANGEMENT OF TUNNEL.

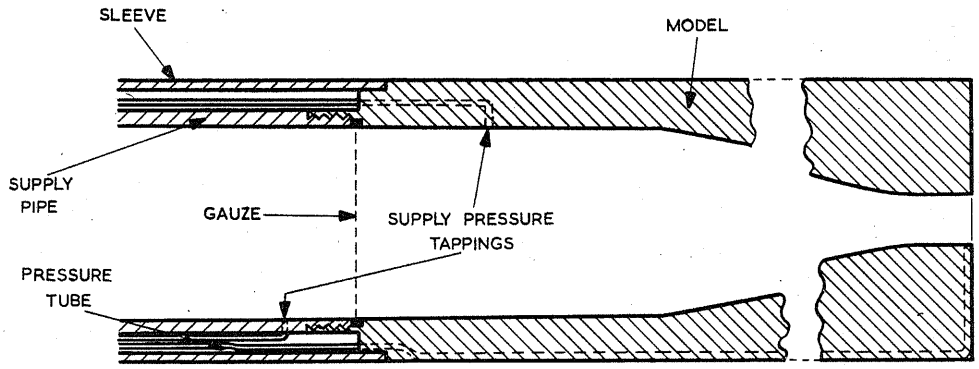

FIG. 2.

DETAIL OF AFTERBODY — PIPE JOINT

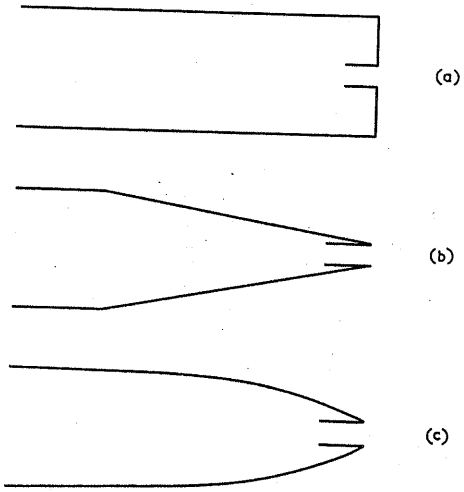

FIG. 3.

THE AFTERBODIES (3/20 scale.)

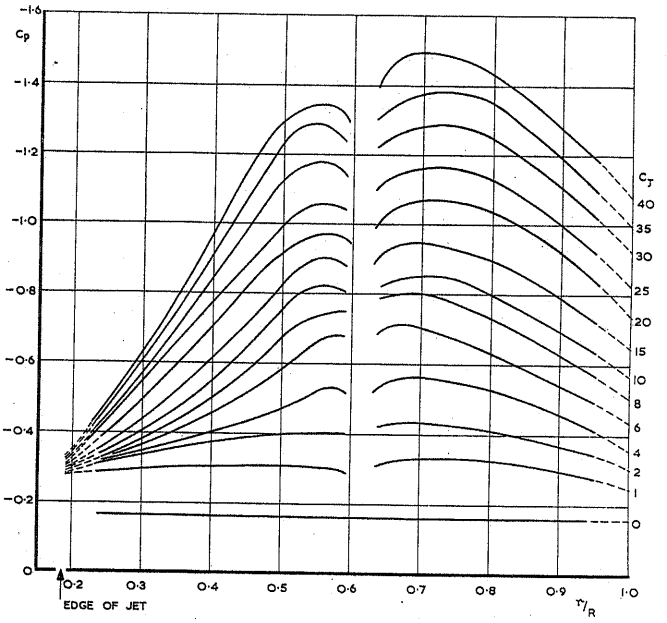

FIG. 4a.

BASE PRESSURE DISTRIBUTION ON RIGHT CYLINDER

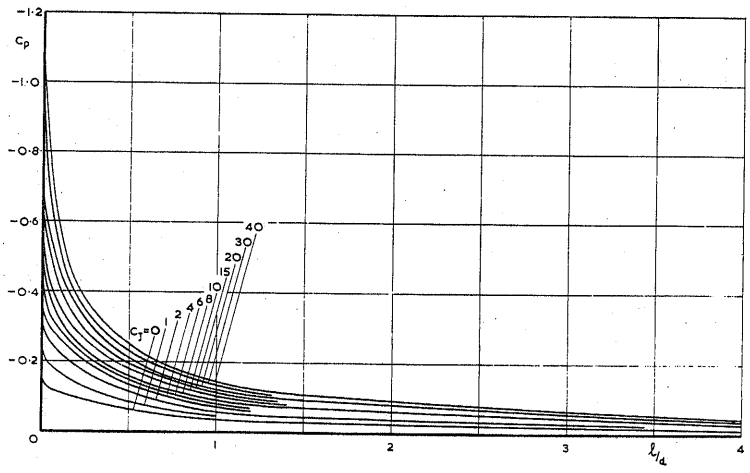

FIG. 4b.

PRESSURE DISTRIBUTION ON SIDE OF RIGHT CYLINDER

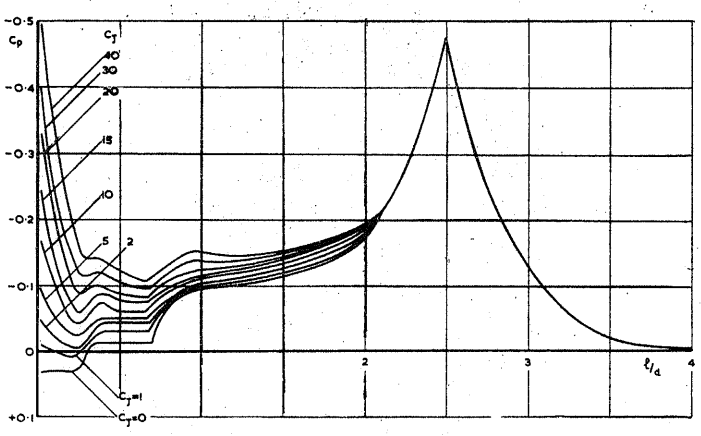

FIG. 5.
PRESSURE DISTRIBUTION ON BOAT–TAIL

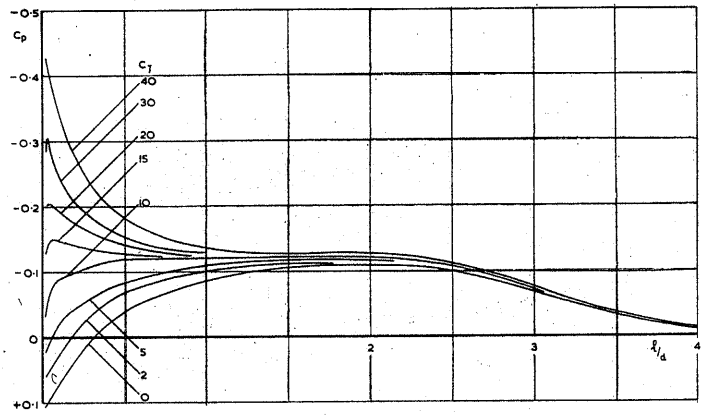

FIG. 6.
PRESSURE DISTRIBUTION ON ELLIPSOID.

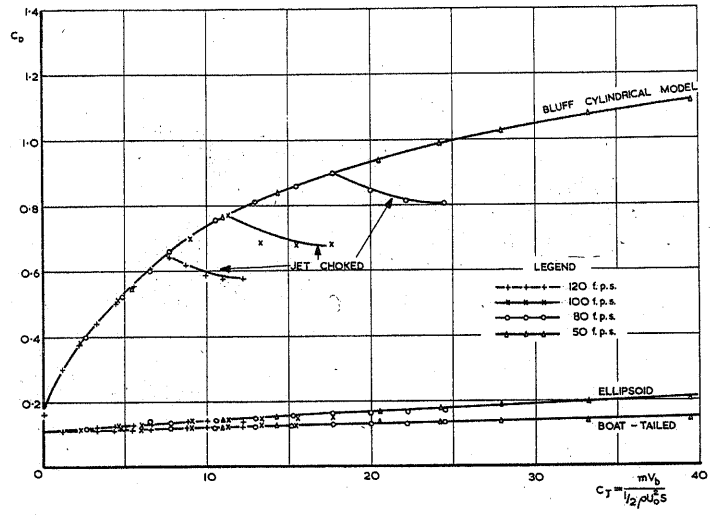

FIG. 7
VARIATION OF C_D WITH C_J

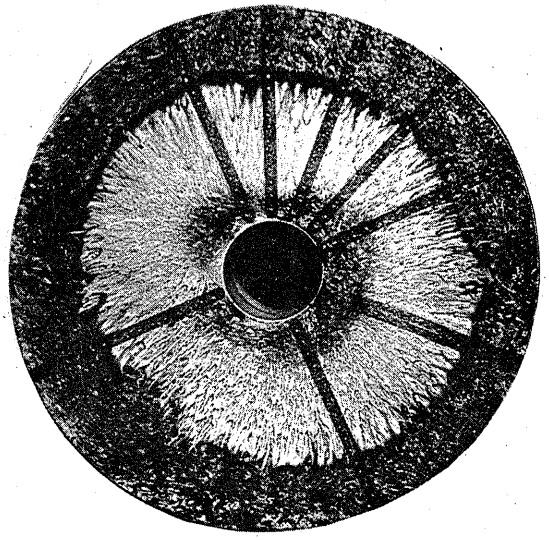

FIG. 8 FLOW PATTERN - BASE OF RIGHT CYLINDER
$C_J = 6$, $U_o = 120$f. p. s.

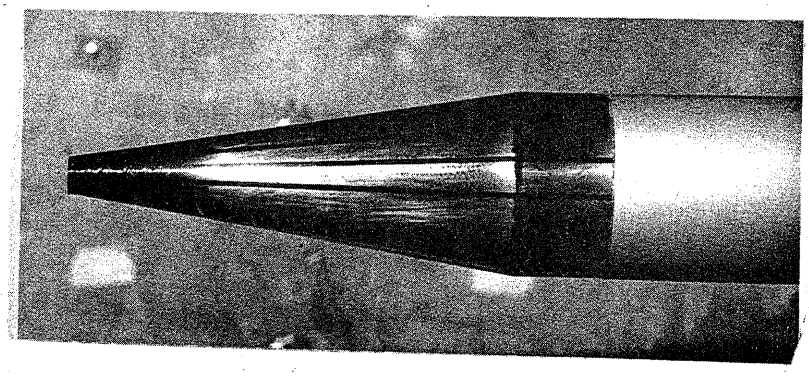

FIG. 9 FLOW PATTERN - TAPERED AFTERBODY
$C_J = 0$, $U_o = 120$ f.p.s.

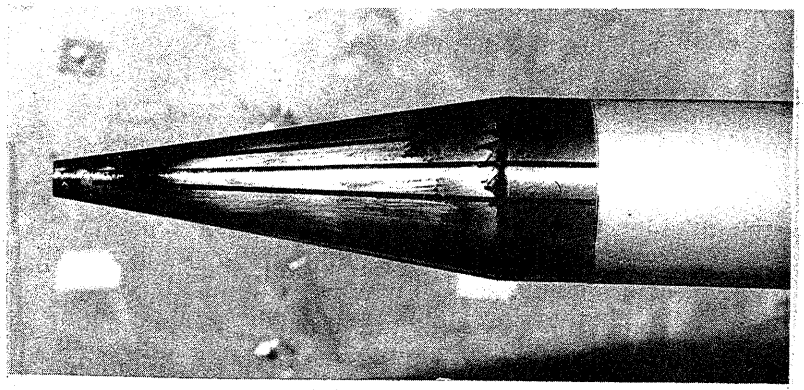

FIG. 10 FLOW PATTERN - TAPERED AFTERBODY
$C_J = 5$, $U_o = 120$ f.p.s.

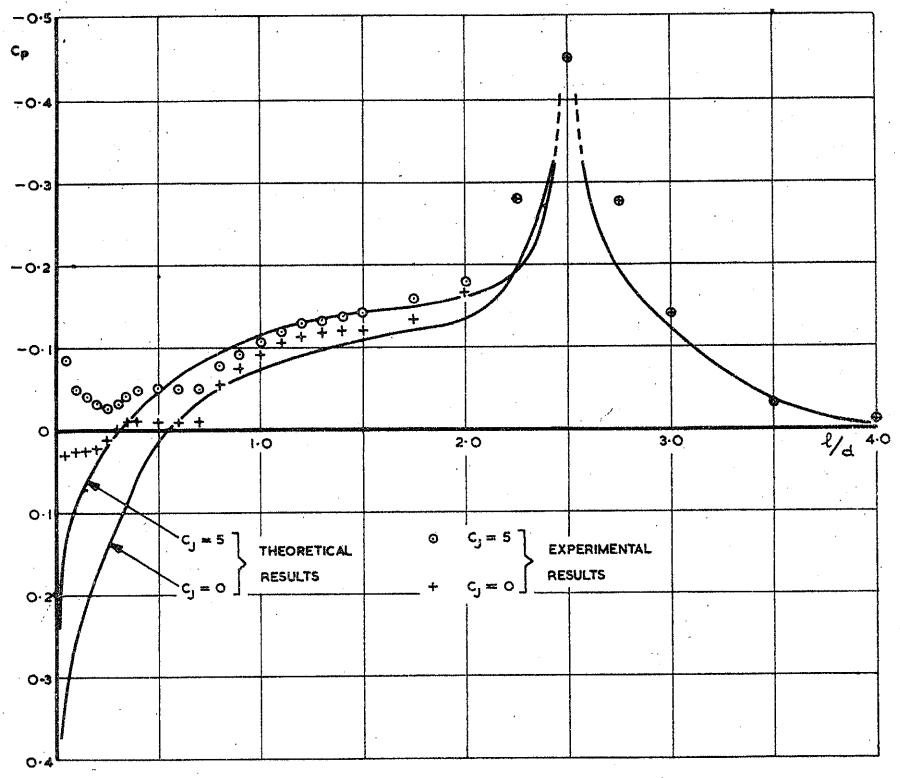

FIG. 11. COMPARISON BETWEEN THEORY & EXPERIMENT; BOAT - TAILED MODEL.

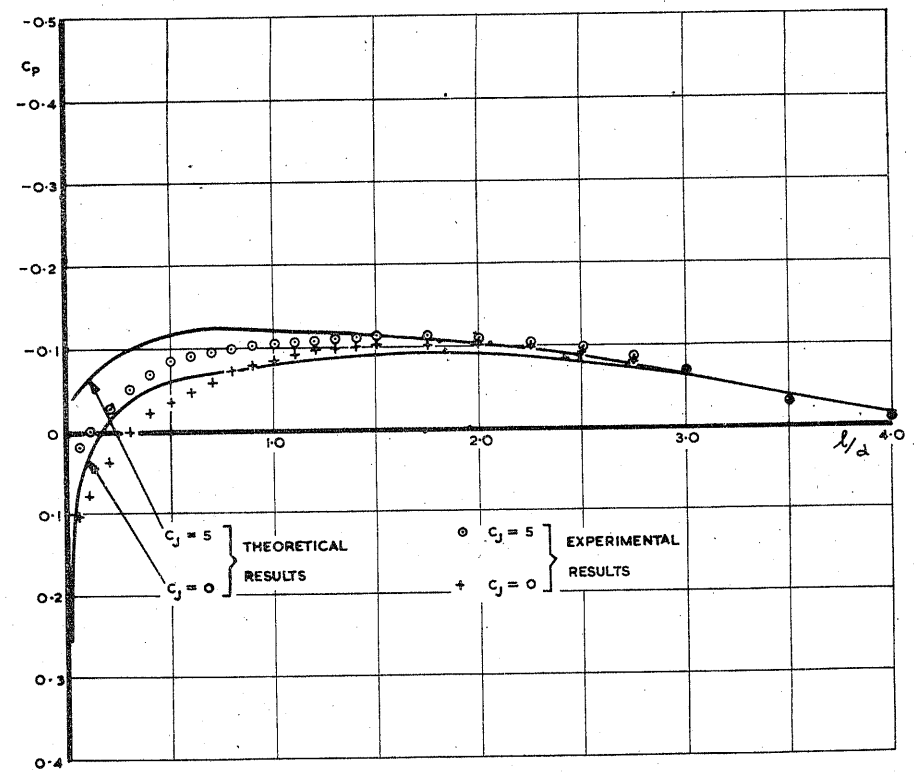

FIG. 12. COMPARISON BETWEEN THEORY & EXPERIMENT — ELLIPSOID.